Approaching detachment in I-mode – Response of Core Confinement and the Edge Pedestal in the ASDEX Upgrade tokamak

T. Happel,[1,*] M. L. Reinke,[2] D. Silvagni,[1,3] M. Bernert,[1] O. Grover,[4] P. Hennequin,[5] A. E. Hubbard,[6] U. Plank,[1] E. Trier,[1] D. Brida,[1] P. David,[1] R. Fischer,[1] L. Gil,[7] K. Höfler,[3,1] P. Manz,[1,3] R. M. McDermott,[1] A. Merle,[8] U. Stroth,[1,3] E. Viezzer,[9] M. Willensdorfer,[1] the ASDEX Upgrade Team,[10] and the EUROfusion MST1 Team[11]

[1]*Max-Planck-Institut für Plasmaphysik, Boltzmannstr. 2, 85748 Garching, Germany*

[2]*Oak Ridge National Laboratory, Oak Ridge, Tennessee 37831, USA*

[3]*Physik-Department E28, Technische Universität München, James-Franck-Str. 1, 85748 Garching, Germany*

[4]*Institute of Plasma Physics, The Czech Academy of Sciences, Prague, Czech Republic*

[5]*Laboratoire de Physique des Plasmas, Ecole Polytechnique, 91128 Palaiseau, France*

[6]*Plasma Science and Fusion Center, Massachusetts Institute of Technology, Cambridge, Massachusetts 02139, USA*

[7]*Instituto de Plasmas e Fusão Nuclear, Instituto Superior Técnico, Universidade de Lisboa, Portugal*

[8]*Ecole Polytechnique Fédérale de Lausanne (EPFL), Swiss Plasma Center (SPC), CH-1015 Lausanne, Switzerland*

[9]*Dept. of Atomic, Molecular and Nuclear Physics, University of Seville, Seville, Spain*

[10]*see the author list "H. Meyer et al., Nucl. Fusion* **59**, *112014 (2019) (https://doi.org/10.1088/1741-4326/ab18b8)"*

[11]*see the author list "B. Labit et al., Nucl. Fusion* **59**, *086020 (2019) (https://doi.org/10.1088/1741-4326/ab2211)"*

(Dated: 2020-12-10)

Abstract

Experiments on nitrogen assisted divertor detachment in the improved energy confinement mode (I-mode) are reported from the ASDEX Upgrade tokamak. When nitrogen is introduced into the divertor and radiation losses cool the divertor plasma down, a loss of core confinement is observed, concomitant with an increase in low frequency edge fluctuation levels. The loss in confinement can be compensated and the I-mode can be maintained by additional heating power input. Detachment of the inner divertor leg has been observed for the first time in an I-mode discharge. The outer divertor leg remains attached in these experiments. Good energy confinement properties ($H_{98}(y, 2) = 0.9$) during the detachment of the inner divertor leg are reported.

*Electronic address: tim.happel@ipp.mpg.de

I. INTRODUCTION

During the last few years, it has become evident that the classical type-I ELMy H-mode regime [1] is only a viable option for a DEMO tokamak if the ELMs are suppressed or mitigated [2]. While ELM mitigation and suppression techniques exist, it is questionable whether the parameter space, in which these techniques are reliably used, is compatible with DEMO requirements. Even for ITER there is concern that unmitigated type-I ELMs might damage the divertor target plates [3].

As a consequence, interest in so-called ELM-free regimes has resurfaced in recent years. These ELM-free regimes can be divided into two categories, *natural* ELM-free regimes (QH-mode [4], I-mode [5–8], EDA H-mode [9–11]) and *suppressed or mitigated ELM* regimes (e.g. through resonant magnetic perturbations (RMPs) [12], vertical kicks [13] or pellet pacing [14]). The natural ELM-free regimes usually develop a characteristic mode in the plasma edge that is believed to keep the edge pedestal away from the peeling-ballooning boundary, so type-I ELMs cannot develop.

However, even ELM-free regimes can still be harmful to the divertor due to stationary heat loads [15–17]. In order to protect the divertor, future reactors will have to rely on a high-confinement plasma scenario that is compatible with a detached divertor. Of the ELM-free regimes mentioned above, only the EDA H-mode has proven (on present-day machines) to meet these criteria [18, 19]. For I-mode, QH-mode and H-mode where ELMs are suppressed by RMPs, the demonstration of compatibility with divertor detachment is one of the key topics of active research. These confiment regimes exhibit high pedestal top temperatures and thus low pedestal top collisionalities. On present-day machines, this is connected to low separatrix density and thus a low separatrix Greenwald fraction, which is disadvantageous for divertor detachment [20]. Therefore, it should be pointed out that an incompatibility with detachment on present-day machines does not necessarily mean that detachment will not be possible in a future reactor, where low pedestal top collisionalities can co-exist with high separatrix Greenwald fractions. Therefore, it would be a significant step forward if detachment of one of the above confinement regimes could be achieved on a present-day machine, even with the limitations mentioned above. The results could be used to make predictions and extrapolations for future devices, which could potentially impact their design and optimization for the desired operational scenario.

Divertor detachment can be obtained by cooling of the divertor plasma to low temperatures, such that volumetric processes become important. Pressure loss due to transport, charge exchange,

and potentially via recombination of plasma ions with electrons lead to a decrease of ion flux to the target. In combination with the increased power losses this entrails significantly reduced directed power fluxes onto the divertor targets. In ASDEX Upgrade, the divertor plasma of typical low-confinement mode plasmas (L-modes) can be cooled and subsequent detachment can be obtained by increasing the plasma density and the neutral gas pressure via fueling [21]. In H-mode, due to the high power fluxes, additionally impurities have to be introduced into the divertor plasma. This leads to additional power dissipation via line radiation such that the temperature reduces sufficiently to activate the aforementioned volumetric processes [22]. It is a general observation in ASDEX Upgrade that the inner divertor detaches first, both in forward and reversed field configurations [21, 23].

I-mode detachment studies are scarce. In experiments on Alcator C-Mod with nitrogen (N) seeding, the I-L back transition always occurred before any sign of divertor detachment [24]. The present paper reports on first results of I-mode divertor detachment experiments from the ASDEX Upgrade tokamak. It is shown that the inner divertor leg has been successfully detached while maintaining good confinement. By means of N seeding, the heat flux onto the inner divertor target is drastically reduced, and detachment is obtained. To our knowledge, this is the first time this has been achieved in an I-mode plasma. However, in the experiments presented here, the outer divertor is still attached. Further work is needed to obtain I-mode with detached inner and outer divertors.

This paper is structured as follows: in Sec.II, the detachment experiments are shown, including the loss of confinement with N seeding and the demonstration of inner divertor detachment. Section III presents kinetic and radial electric field profiles and edge turbulence behavior, followed by a summary and conclusions in Sec. V, which includes an outlook to future experiments.

II. NITROGEN SEEDING EXPERIMENTS IN I-MODE

The experiments have been performed in the ASDEX Upgrade tokamak (AUG) [25] in reversed plasma current and magnetic field configuration using the lower divertor. In this configuration, the ion grad B drift points away from the active X-point and the I-mode can be obtained if a threshold in heating power $P_{\mathrm{L-I}}$ is surpassed [8, 26–28]. Two different combinations of magnetic field strength and plasma current have been explored, see Tab. II. The use of the lower divertor in AUG is beneficial for detachment studies since it is a closed divertor with significant neutral

B_t (T)	I_p (MA)	q_{95}	f_{GW}
2.35	-1.0	-4.1	0.31
2.50	-0.8	-5.4	0.35
2.50	-0.8	-5.4	0.44

TABLE I: Parameter space covered in I-mode detachment experiments.

compression and optimized diagnostic coverage [29].

The I-mode response to nitrogen (N) seeding was investigated in two different ways: (i) at constant heating power, (ii) with feedback control to maintain a pre-defined value of the poloidal plasma beta, β_{pol}. The latter method was first applied to obtain stationary neutral-beam injection (NBI) heated I-modes on AUG [30]. **In all cases reported here, N was introduced through a gas inlet valve under the divertor roof baffle. Flow rates were on the order of $1 - 5 \times 10^{21}$ electrons per second. The N concentration in the plasma reached only roughly 1.5%, which implies good impurity screening. Due to mostly non-stationary conditions, no estimates of divertor enrichment [31] and compression [32] can be given.**

Figure 1 shows time traces of four plasma discharges with different N seeding levels. The black traces show the reference discharge without N seeding: a constant electron cyclotron resonance heating (ECRH) power of 2 MW is applied starting at 1.5 s (Fig. 1(a)). The core and peripheral line-average densities remain constant throughout the discharge (b). The L-I transition takes place at $t = 1.78$ s for all cases, which underlines the reproducibility of the experiments performed. The transition can be recognized in the panels showing the pedestal top electron temperature (c), the energy confinement time τ_{E} (d), and the confinement improvement factor $H_{98}(y, 2)$ [33] (e). The pedestal top electron temperature is measured at $\rho_{\mathrm{pol}} = 0.95$ with an electron cyclotron emission (ECE) diagnostic [34]. Here, ρ_{pol} is the square root of the normalized poloidal flux radius. The plasma is optically thick for ECE radiation at this radial position (optical thickness $\tau \approx 7$), which means that the radiation temperature measured by ECE corresponds to the electron temperature. During the L-I transition, the energy confinement and the temperature increase, while the density is unaffected, which is typical for the I-mode confinement regime. The gas puffs for the different discharges are shown in panel (f). The D fueling rate changes slightly because it is feedback controlled on the line-average density. The dashed lines show the N fueling rate, which is zero in the reference discharge (black). The N seeding starts at a low level of 1.5×10^{21} $\mathrm{e^{-}s^{-1}}$ in #35797 (red) at 2.4 s, and it is increased by a factor of 3 at 2.9 s. Shortly after the second step in N seeding,

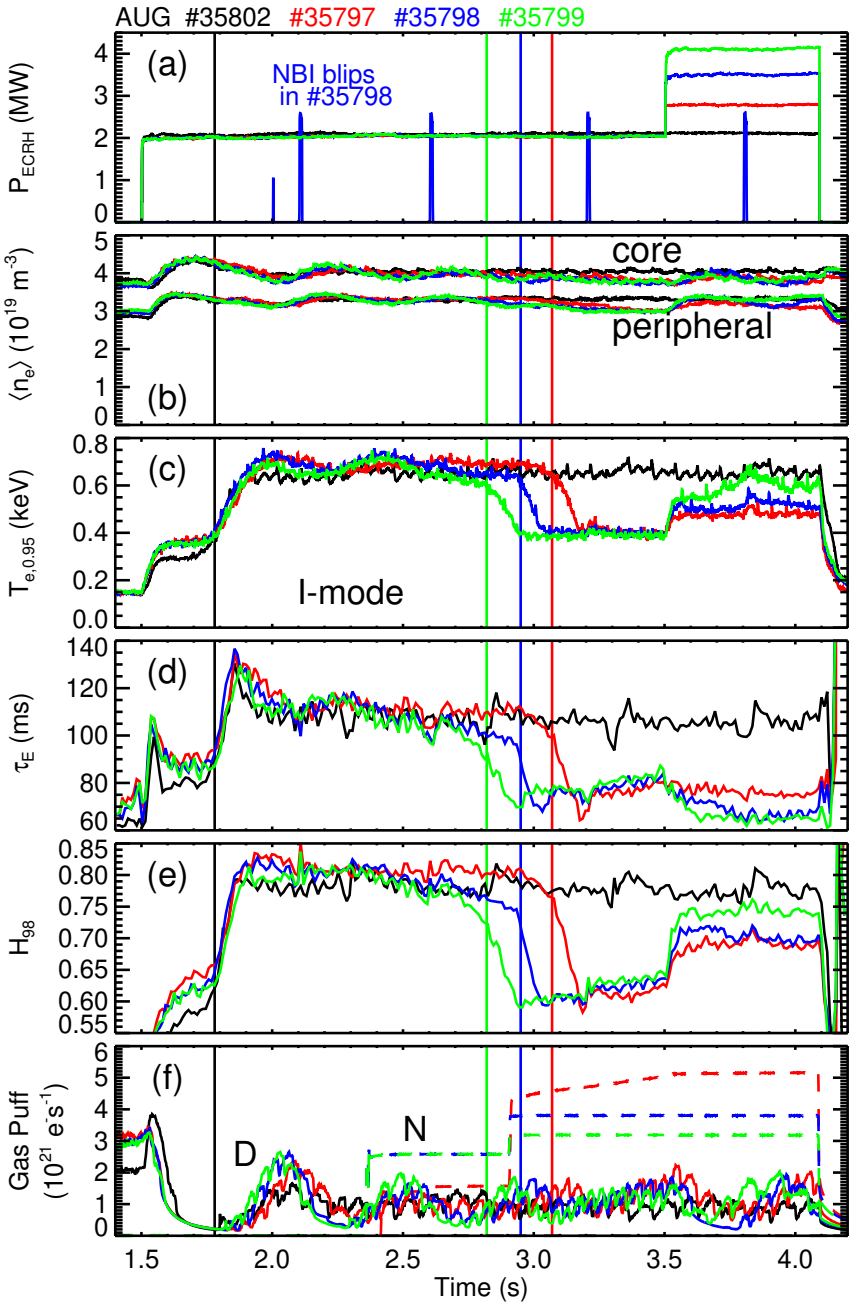

FIG. 1: Time traces of plasma parameters during I-mode detachment experiments. For all cases, $B_t = 2.5\,\mathrm{T}$ and $I_p = -1.0\,\mathrm{MA}$. For details, refer to the text.

the pedestal top electron temperature and the confinement start to decrease until at $t_{\mathrm{I-L}} = 3.08\,\mathrm{s}$, an I-L back transition takes place, indicated by the vertical red line. After this back transition, L-mode parameters comparable to those before the L-I transition are obtained. In the subsequent discharge, #35798 (blue), the puff rate at the first step is higher than before, and the I-mode is lost earlier (at $t_{\mathrm{I-L}} = 2.95\,\mathrm{s}$, vertical blue line). For the last discharge, #35799 (green), the I-L back

transition occurs even earlier ($t_{\mathrm{I-L}} = 2.83\,\mathrm{s}$, vertical green line), which can be attributed to the remaining N inventory from the previous two discharges. The τ_{E} loss from I-mode to L-mode is about 30%. Note that even before the I-L back transition, a gradual confinement loss is observed together with the N seeding (Fig. 1(d)).

The loss of the I-mode as seeding is added to the discharge is a robust effect, and these observations are consistent with results obtained at Alcator C-Mod [24]: N seeding seems to have a deleterious effect on the confinement of the I-mode, leading to lower pedestal top temperatures and lower plasma beta, and ultimately, the I-L back transition is observed. **Both the C-Mod and AUG system fueled N into the private flux region. As described in [24], the C-Mod experiments devoted substantial experimental time to try and manipulate the flow rate of impurities to avoid the I-L back-transition. On C-Mod, main-chamber Ne seeding also led to an I-L back-transition when injected in amounts that were necessary for divertor dissipation. Considering these prior C-Mod results and the qualitatively similar behavior shown in Fig. 1 in the initial AUG experiments, the focus of subsequent AUG plasmas shifted to using different investigative approaches that were unavailable to C-Mod such as modifying the mix of ion and electron heating as well as β_{pol} feedback control of input power (shown later).**

In all N-seeded discharges in Fig. 1, more central ECRH power is added at 3.5 s into the second L-mode phase of the discharge (panel (a)). It is not possible to return to I-mode or to reach H-mode, even for doubled auxiliary heating power (#35799). The pedestal top T_e **increases about 40% with respect to the L-mode phase before heating is added**, but the energy confinement time drops slightly. **The pedestal top T_i increases only by about 10%. This has the consequence that the edge E_r does not deepen significanly with respect to the L-mode value from the phase before, which is confirmed by Doppler reflectometry measurements (not shown here). It is known that a sufficiently deep edge E_r well is required in AUG to access H-mode [35], which cannot be achieved with the additional ECRH heating applied here**. The confinement improvement factor $H_{98}(y,2)$ increases somewhat. This is due to the fact that $H_{98}(y,2)$ is scaled to reflect the power degradation of the H-mode ($\propto P^{-0.69}$), but the plasma under consideration is in L-mode which has less power degradation ($\propto P^{-0.50}$, see Ref. [36]). The reason why the discharges **do not return into I-mode** with this additional power step is unclear at the moment**, although it could be speculated that the missing pedestal top ion temperature increase could play a role for the L-I transition [37]**. With the additional power step in #35798 and #35799, the core plasma radiation is reduced (not shown), which is indicative of higher impurity transport

levels [38]. It is possible that strong transport is active during this phase of the discharge, as also the energy confinement time (panel (d)) drops with this additional power step. **This observation is of particular importance, and it will be followed up with dedicated studies in the future**.

Two main points become clear from the previous observations: first, N seeding during an I-mode discharge causes the confinement to drop, resulting eventually in an I-L back transition. This is not because of increased core radiation, as will be shown later. Instead, it seems likely that the core and/or the edge transport increases. For this reason, the reaction of edge density turbulence to the seeding will be investigated in Sec. III. Second, additional auxiliary heating is unable to bring the plasma back into an I-mode or H-mode. In the following, the plasma energy loss is counteracted with the use of neutral beam heating. Furthermore, the heating power is feedback controlled via a β_{pol} controller. This has the effect that a loss in plasma energy due to a loss in confinement quality can be compensated with additional heating power, which can potentially maintain the I-mode confinement regime during N seeding.

The resulting plasma behavior is analyzed further in Fig. 2. The request value and the actual value of β_{pol} is plotted in (e). At $t = 2.8\,\mathrm{s}$, I-mode begins, which is seen in the increase in the energy confinement time τ_{E} (d), the reduction of NBI heating power P_{NBI} (a), and the development of the so-called weakly coherent mode (WCM) [8, 39–41] at roughly 80 – 100 kHz as measured by reflectometry with a homodyne detection scheme [42] at $\rho_{\mathrm{pol}} = 0.985$ (g). Note that, in order to put emphasis on the WCM, the color scale in (g) has been adjusted accordingly. The WCM is usually observed in I-mode and as such is a good indicator of the I-mode confinement regime, although it has been observed that the WCM can also exist in L-mode, albeit at lower frequency [30]. The reduction of P_{NBI} is caused by the β_{pol} feedback: since the energy confinement time increases as I-mode is entered, less power is necessary to maintain the same value of β_{pol}. The density remains constant during the entire time window (not shown). The N puff starts at $t = 4.0\,\mathrm{s}$ and increases linearly until it reaches a final value of $3.2 \times 10^{21}\,\mathrm{e^-s^{-1}}$ (panel (f)). Together with the N puff, τ_{E} decreases, and the resulting loss in plasma beta (panel (e)) is compensated by increasing the NBI power (panel (a)). During this phase, β_{pol} remains within 2% of its target value. At $t = 5.45\,\mathrm{s}$, the I-mode is lost, which is seen in the sudden drop of τ_{E} and in the disappearance of the WCM. Furthermore, the NBI power is increased by the feedback system in order to maintain the value of β_{pol}. During this time window, the core radiation (panel (b)) barely increases while the divertor radiation does react to the N seeding, as obtained from tomographic reconstruction [43] and spatial integration of bolometer data. This is seen particularly well in the later L-mode phase, in which

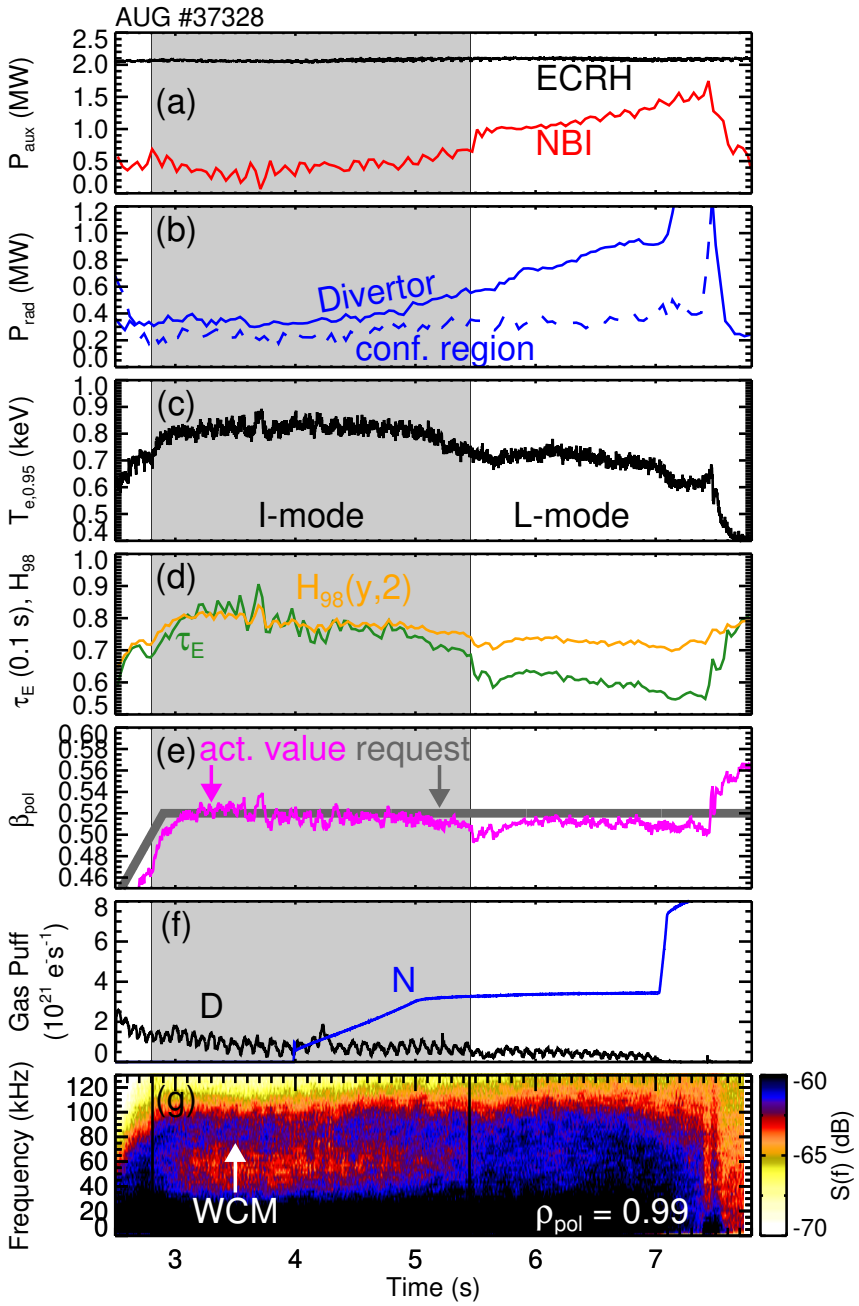

FIG. 2: Time traces of plasma parameters during a N-seeded I-mode. Although the auxiliary heating power is controlled via β_{pol} feedback, an I-L transition occurs at 5.45 s. For details, refer to the text.

the radiation from the divertor, $P_{\mathrm{rad,div}}$, is significantly higher than that from the core, $P_{\mathrm{rad,core}}$.

Usually, I-mode is situated between L-mode and H-mode in terms of β_{pol} [28, 30]. Although the feedback system is capable of maintaining β_{pol}, the I-mode confinement regime is lost through a transition into L-mode at 5.45 s. This leads to the question as to whether I-mode is incompatible with strong divertor radiation or if it can be recovered. In fact, Figure 3 shows that also strongly

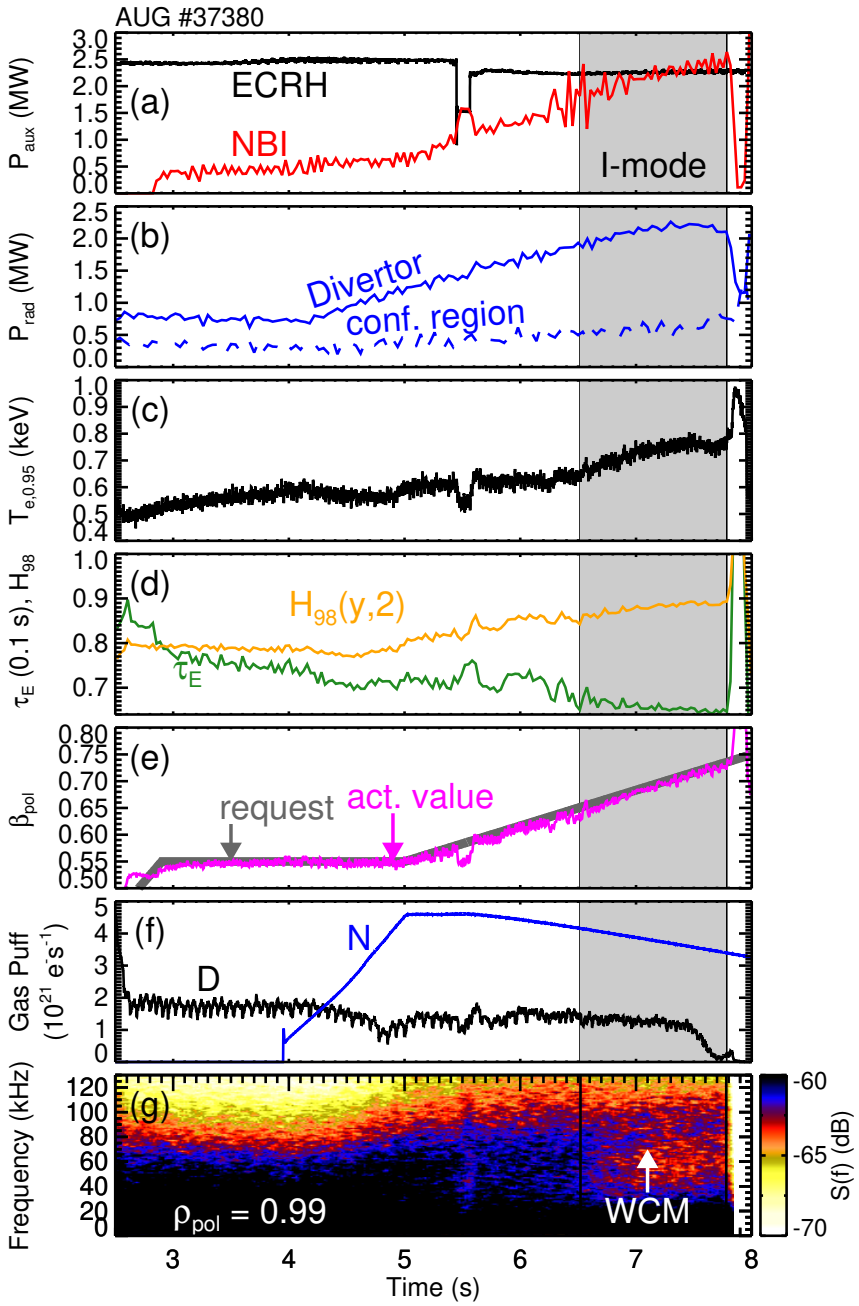

FIG. 3: Time traces of an L-I transition during strong N seeding, in which the divertor radiation is significant (b). The auxiliary heating was controlled via β_{pol} feedback. Detachment is obtained between 4.92 and 7.52 s, I-mode between 6.52 and 7.82 s. For details, refer to the text.

N-seeded I-modes can indeed exist, however at elevated values of β_{pol} compared to non-seeded I-modes.

The N puff starts at $t = 3.95$ s into an L-mode plasma (Fig. 3(f)). A β_{pol} feedback ramp is started at $t = 5$ s (e). The effect of the heating ramp is seen in panels (a) and (c), where in (a)

the NBI power is ramped and in (c) the pedestal top electron temperature, $T_{e,0.95}$, increases. Since the heating power is ramped during an L-mode, which usually shows has less power degradation than H-mode [36], the confinement improvement factor $H_{98}(y, 2)$ is comparably high even during this phase of the discharge. At 6.3 s, there is a pronounced increase in $T_{e,0.95}$. This is when the I-mode starts, which is also seen in the development of a WCM (Fig. 3(g)). During this phase, the confinement improvement factor $H_{98}(y, 2)$ increases further and reaches a value of 0.9 (d). While the core radiation is comparably low, the divertor radiation increases substantially during the N seeding phase (Fig. 3(b)).

In this discharge, the inner divertor is detached between 4.92 and 7.52 s, i.e. there is a phase in L-mode with detached inner divertor, and the plasma enters I-mode during this detached state at 6.52 s. This clearly demonstrates that I-mode is compatible with detached divertor conditions, at least for one detached divertor leg. At 7.52 s, the plasma re-attaches, and at 7.82 s, a transition to H-mode takes place. It is worth noting that in contrast to the discharges in Figs. 1 and 2, this plasma does go into H-mode as the heating power is increased. The most prominent difference is that here, an I-H transition takes place, while the plasma had undergone an I-L back transition and remained in L-mode in Figs. 1 and 2, even at increased auxiliary heating power. This different behavior related to L-H and I-H transitions in N seeded discharges is not understood at the moment. Furthermore, it should be pointed out that the value of β_{pol} during the I-mode phase is between 0.63 and 0.74, which is significantly higher than in the non-seeded case (0.50 – 0.60).

Several divertor properties for this discharge are displayed in Fig. 4. Panels (a-c) depict inner target temperature, target density and heat flux density inferred from measurements by Langmuir probes and infrared cameras, respectively. Panels (d-f) depict the same quantities for the outer divertor. The coordinates s_{inner} and s_{outer} are coordinates along the divertor tiles. In order to infer the heat flux density onto the divertor for (c) and (f), the heat diffusion equation is solved inside the tile for all time points during the discharge [44, 45]. The detachment of the inner divertor is seen in the fast drop of the target temperature to ~ 5 eV at a distance of 3 cm from the strike point (SP) (panel (a)). During this time, the target plasma density increases slightly to 2×10^{19} m^{-3}. The heat flux to the divertor vanishes, and only re-appears once detachment is lost at 7.52 s. Therefore, one can conclude that the inner divertor is detached. In contrast, the outer divertor remains attached during the whole discharge, although a slight reduction of target temperature (panel (d)) is observed during the N seeding interval close to the strikepoint (SP). Towards the end of the discharge, it seems as if a second lobe appears in the outer divertor heat flux data in panel (f). This

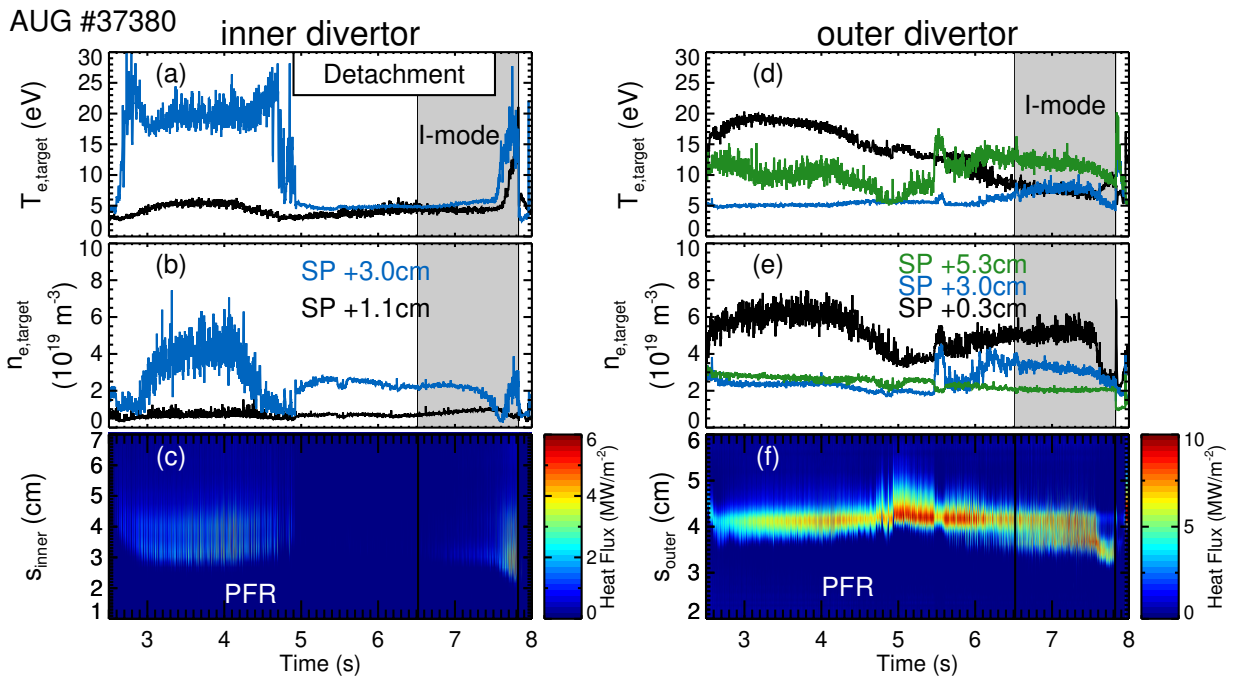

FIG. 4: Evolution of divertor properties during L- and I-mode detachment of the inner (a-c) and outer divertor (d-f). Inner divertor detachment is achieved at 4.92 s, as the drop in the inner divertor target temperature (a) and the drop in heat flux (c) indicate. Differently colored time traces indicate distances from the strike point (SP). For details, refer to the text.

is due to an enhanced emissivity of the region around $s_{\text{outer}} \approx 4\,\text{cm}$.

The poloidal radiation distribution in three different phases of the discharge ((a) L-mode with inner divertor detached, (b) I-mode with inner divertor detached, (c) I-mode, attached) is presented in Fig. 5. In both detached L- and I-mode, the inner divertor shows a strong radiation pattern close to the strikepoint. Note that the stronger radiation in I-mode is most likely due to the increased input power during this phase of the discharge, see Fig. 3(a). The radiative region vanishes almost entirely as the plasma re-attaches (c). Although a strongly radiative outer divertor is observed as well, the radiated power is not sufficient to cool the divertor plasma down to temperatures where detachment sets in ($\sim 5\,\text{eV}$). In particular, no significant radiation is present in the confined plasma, confirming the statement from Fig. 3(b). This supports the conclusion that the confinement loss as N is introduced is linked to increased edge transport, possibly in conjunction with the low-frequency turbulence increase as shown in Fig. 2(g) and in the next section in Fig. 8.

To summarize, several key observations are reported: (i) I-mode operation is compatible with at least one detached divertor leg, (ii) the introduction of N into the private flux region leads to a

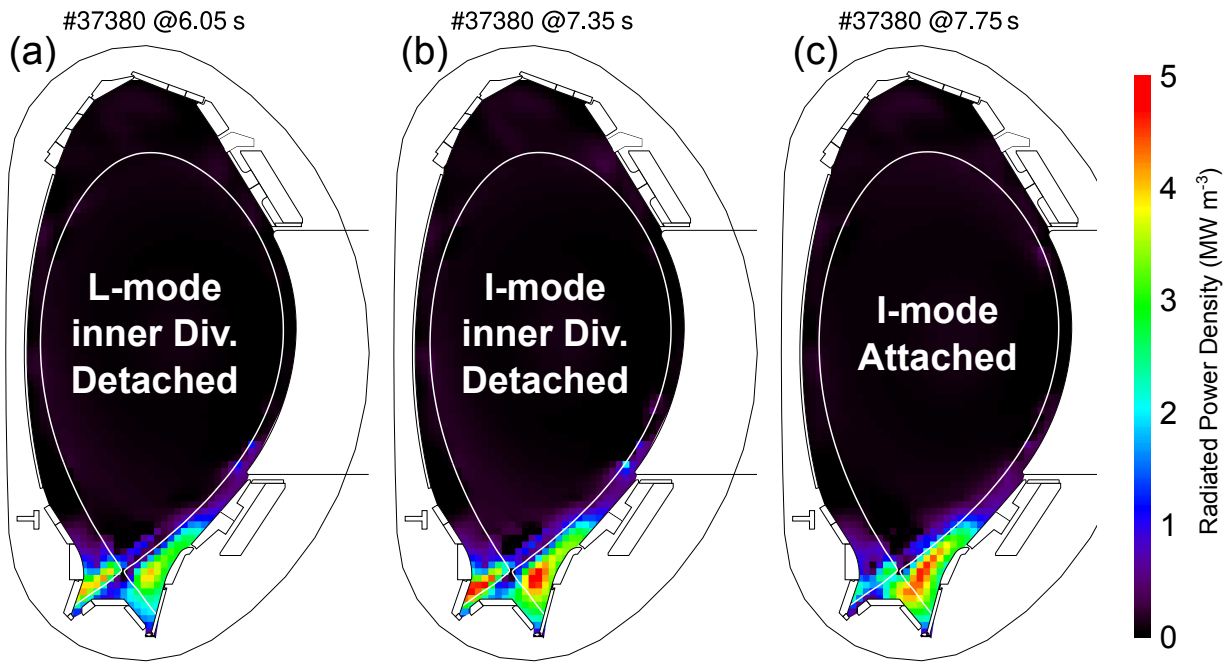

FIG. 5: Tomographic reconstruction of radiation measured by foil bolometers for L-mode with detached inner divertor (a), I-mode with detached inner divertor (b) and attached I-mode (c). The radiation present at the inner divertor leg disappears as the plasma re-attaches. No X-point radiator is observed.

loss in confinement, (iii) this loss in confinement can be very pronounced such that even doubled heating power does not bring the plasma back into I-mode. Since the edge turbulence behavior (cf Fig. 2 and later, Fig. 8) is affected by N seeding, it seems likely that the loss in confinement comes from the edge. Therefore, in the following, edge profiles and fluctuations are analyzed.

III. THE PLASMA EDGE DURING N SEEDING

In the previous section, a confinement loss during N seeding into an I-mode plasma has been observed without any increase in core radiation, which hints to increased edge transport. Therefore, this section presents kinetic and radial electric field profiles and fluctuation measurements during seeding.

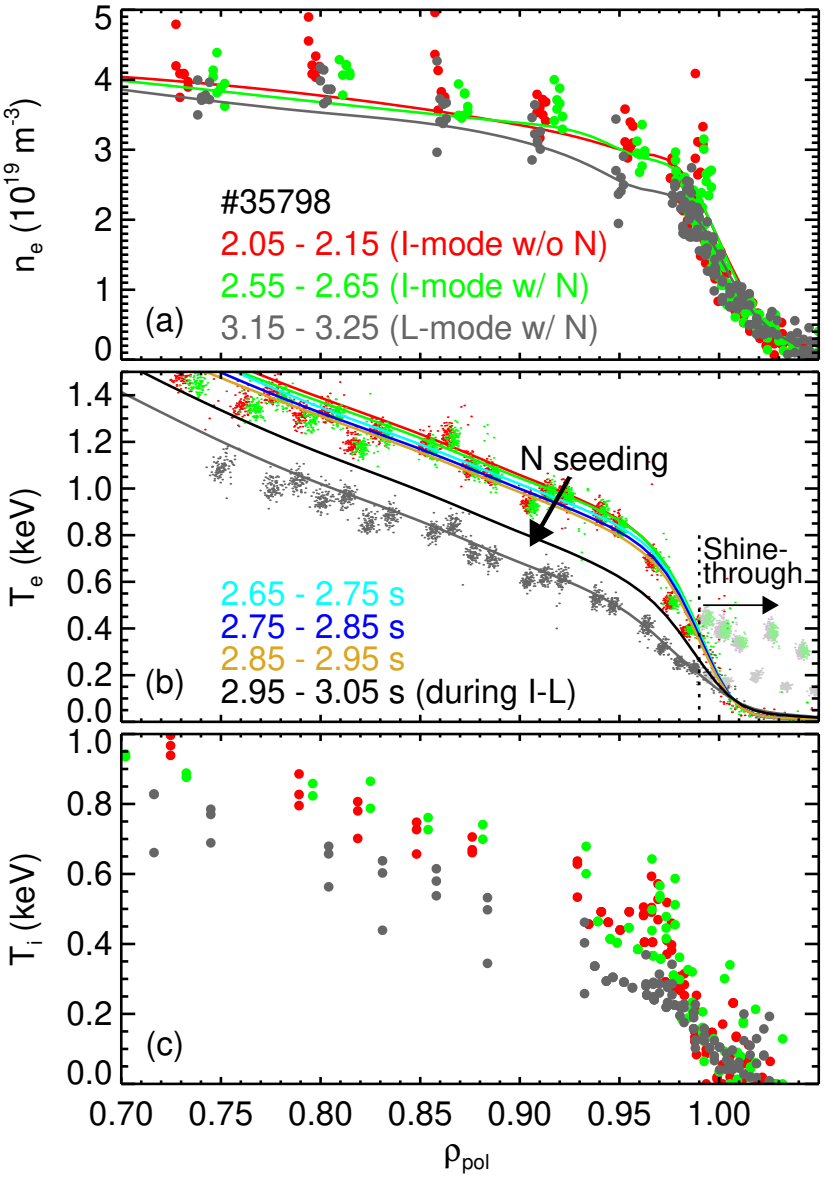

FIG. 6: Edge profiles of electron density (a), electron temperature (b) and ion temperature (c) for different time points (colors) during N seeding.

A. Kinetic Profiles

Figure 6 depicts edge kinetic profiles of electron density (a), electron temperature (b), and ion temperature (c) at different time points in discharge #35798, the discharge in Fig. 1, where a loss of I-mode confinement quality is observed during N seeding, followed ultimately by an I-L back transition. The lines in Fig. 6 are obtained via the integrated data analysis (IDA) framework based

on Bayesian inference of diagnostic data [46]. Density and electron temperature profiles are measured with a Thomson scattering diagnostic [47]. The electron temperature profiles also include data from an electron cyclotron emission (ECE) diagnostic [34], and ion temperature profiles in (c) have been obtained with charge exchange recombination spectroscopy (CXRS) [48, 49].

The three density profiles are from three different time windows in the discharge, I-mode without N seeding (2.05 – 2.15 s), I-mode with N seeding (2.55 – 2.65 s), and L-mode with N seeding (3.15 – 3.25 s). There is a slight difference in pedestal top density ($\rho_{\mathrm{pol}} = 0.90 - 0.97$) between L-mode and both seeded and non-seeded I-mode (Fig. 6(a)). Since the density in this discharge is feedback controlled, it seems unlikely that this is due to an increased influx due to recycling, but rather a slight change in pedestal particle transport that sets a different boundary condition at the pedestal top. Note that these changes are small, but so far seem to consistently occur between L-mode and I-mode on AUG [28].

The electron temperature, T_e, profiles (Fig. 6(b)) show a clear pedestal in I-mode, as is usually observed. Apart from the profiles at the time points in (a), additional T_e profiles are included at various times during the N seeding into the I-mode. With evolving time, the pedestal top temperature is reduced, until at 2.95 s, the I-L back transition occurs. This is in agreement with a loss in energy confinement at constant heating power. The core density profile gradient is unchanged, which points towards an increased plasma edge electron heat transport as N is introduced into the private flux region. The measurements at $\rho_{\mathrm{pol}} > 0.98$ are subject to ECE shinethrough. However, the temperature profiles from IDA take this effect into account [50] and are also constrained by Thomson scattering measurements, resulting in almost identical electron temperature profiles in the SOL.

Profiles of the ion temperature are shown in Fig. 6(c), where the energy confinement increase in I-mode with respect to L-mode is also reflected. Only three NBI blips for CXRS measurements were applied in this discharge, so the detailed evolution of ion temperature profiles during seeding cannot be deduced. The I-mode profiles cannot be distinguished within their uncertainties. The profile with seeding was measured between 2.55 and 2.65 s, where also in the electron temperature almost no effect is visible yet.

The profiles from discharge #37380, which features a transition from an L-mode with detached inner divertor into an I-mode with detached inner divertor (cf figs. 3 and 4), are shown in Fig. 7. Throughout the discharge, the density stays constant (a). The electron (b) and ion (c) temperatures are increased with respect to the values of L-mode. Note, however, that during this discharge, an

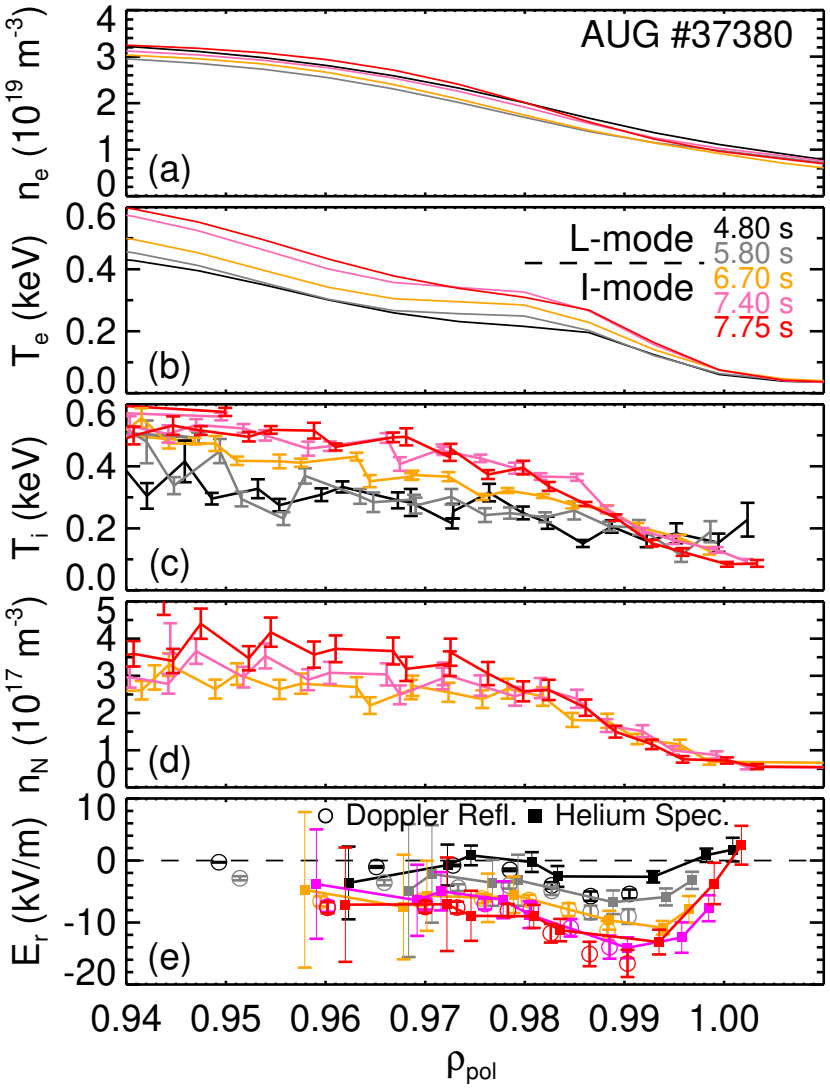

FIG. 7: Edge profiles of electron density (a), electron temperature (b), ion temperature (c), N impurity density (d) and edge radial electric field (e). Throughout N seeding, both electron and ion temperatures increase due to increased auxiliary heating power, while the N impurity density barely increases. The edge radial electric field well deepens to roughly −15 kV/m.

NBI heating ramp is applied (cf Fig. 3(a)), such that the temperature increase is a consequence of both increased confinement and increased auxiliary heating power. Nevertheless, it is clear that the pedestal top temperature increases for both ions and electrons. This increase is also observed towards the plasma center, which reflects the overall increase in plasma energy. The N content is monitored in Fig. 7(d), measured with charge exchange recombination spectroscopy [51]. At the pedestal top it evolves from roughly 1 % at the beginning of the discharge to about 1.5 % at the

end. These values for the concentration are also observed in the plasma center (not shown here) and are comparable to values observed previously during H-mode detachment experiments [23].

Figure 7(e) displays the radial electric field as measured by active spectroscopy of He II [52] and Doppler reflectometry [53, 54], where the latter is based on the assumption that the turbulence phase velocity is small compared to the $E \times B$ velocity, which is usually the case in fusion plasmas [55–60], although some exceptions have been reported [53, 61, 62]. There is good agreement between He spectroscopy and Doppler reflectometer measurements, which overlap in the edge plasma region. It is apparent that the I-mode edge radial electric field well is somewhat deeper than the L-mode values, as observed previously [27, 63–65]. The profile just before the I-H transition (7.75 s) shows a well depth of roughly -15 kV/m. At a magnetic field strength of -2.5 T, this value is consistently observed in non-seeded I-mode discharges just before the I-H transition on AUG [27, 64], and also in L-H transitions in favorable configuration [35, 66]. These measurements support the general observation that at some threshold value of the E_r shear (or flow shear), a transition to H-mode takes place, regardless of whether favorable or unfavorable magnetic configuration is used. In fact, the data here suggest that the unfavorable configuration keeps the E_r shear from reaching its threshold value for the transition into H-mode. Taking this conjecture further, it seems likely that the radial electric field does not play a central role in I-mode physics, an experimental observation that supports recent results from theory and simulation work [37].

B. Fluctuations During Nitrogen Seeding

In Sec. II it was observed that the edge density fluctuation spectrum was modified as nitrogen was introduced into the discharge. This effect is quantified in more detail in Fig. 8, where the fluctuations obtained with an antenna of the poloidal correlation reflectometry system [67] are bandpass-filtered in different frequency bands and the fluctuation powers **relative to the fluctuation power in the WCM frequency range (70 – 140 kHz)** are plotted in panels (a) to **(c)**. **The diagnostic measures poloidal turbulence wavenumbers in the range $k_\theta = 0$ – 3 cm^{-1}, which includes the WCM at $k_\theta \approx 1.5$ cm^{-1} [40, 41].** The black lines show the discharge with N seeding, while the grey lines show the reference discharge from Fig. 1 without N seeding. In the reference discharge, the I-mode starts at the same time (1.78 s) and continues for the rest of the time frame. The frequency bands have been chosen according to the general shape of I-mode spectra: the WCM is in the range 70 – 140 kHz. **The low frequency part is separated into a very low fre-**

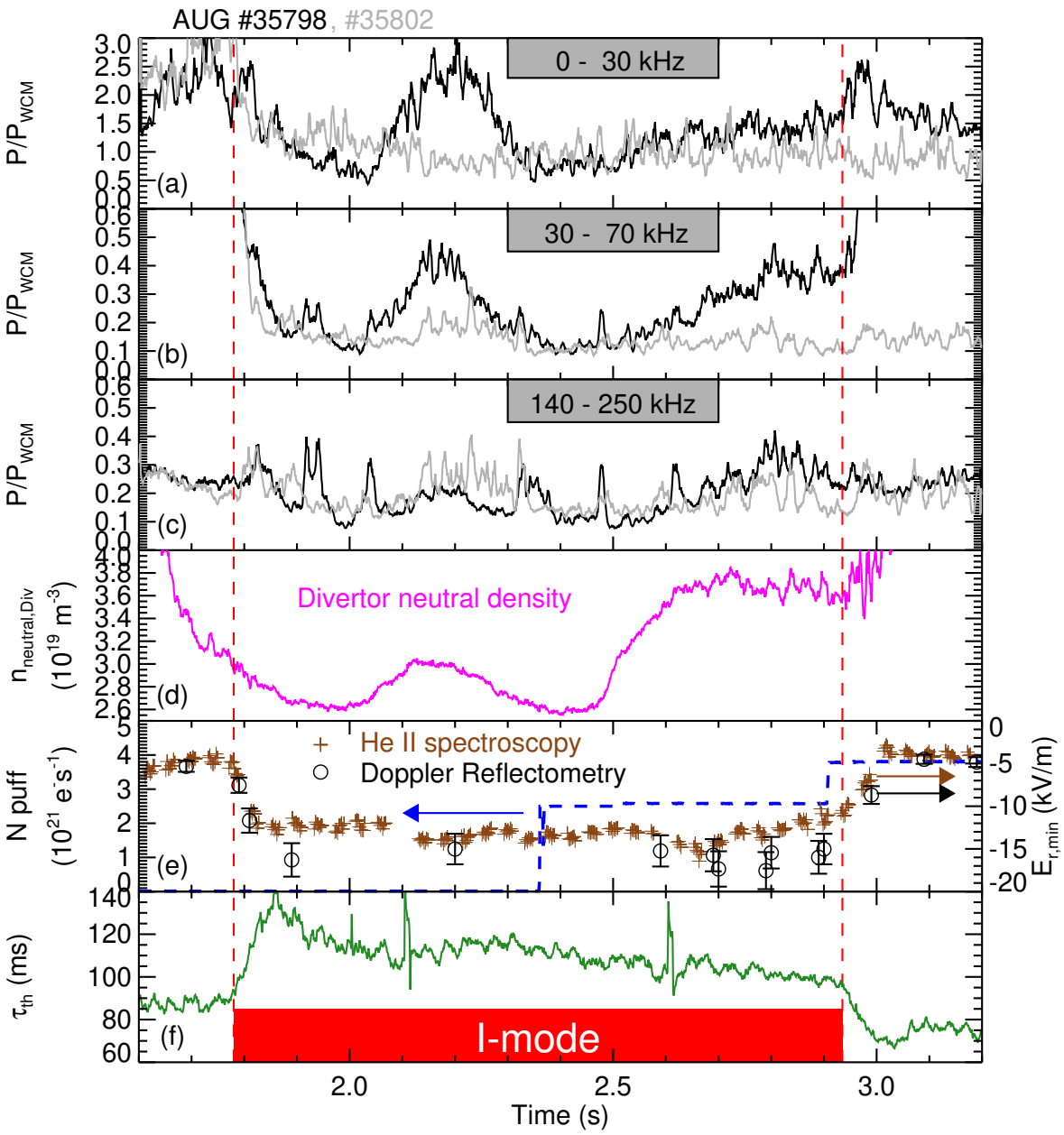

FIG. 8: Density fluctuation power in different frequency bands (a – d) reacting to N seeding (e). The energy confinement time (f) decreases as N is added to the discharge (cf Fig. 1). For reference, fluctuation powers from a non-seeded comparison discharge are shown (grey, a – d).

quency component (0 – 30 kHz, (a)) and the frequency band up to the WCM frequency (b). The higher frequencies (140 – 250 kHz) are shown in (c). The divertor neutral density is plotted in (d), the N seeding rate is plotted in (e) (dashed, blue), and the thermal energy confinement time in (f). Just before and throughout the L-I transition, low-frequency fluctuation levels between

0 and 70 kHz are reduced. Generally, there is little power in the high frequencies from 140 – 250 kHz (c)**. This can be expected from a spectrum of two-dimensional turbulence, where turbulence is free to develop. This is typically the case in fusion plasmas, where the power decays from low towards high frequencies [68–71]. As in the I-mode case, where power is injected close to the WCM frequency, power is expected to decrease from the WCM frequency towards higher frequencies [37]**. Just as I-mode is entered, the high-frequency fluctuation powers are increased, which could be caused by the spin up of the edge plasma (cf panel (e)). This increased flow velocity will cause large-scale fluctuations – which usually contain higher fluctuation amplitudes – to appear at higher frequencies. **A pronounced increase of low-frequency fluctuations is visible between 2.0 and 2.3 s. The exact reason for this has not been determined yet. However, this increase is strongly correlated with an increase in divertor neutral density (panel (d)). Since divertor conditions can determine separatrix parameters [37, 72], it could be speculated that this change in divertor neutral pressure is tied to the fluctuation level increase observed by reflectometry.** During N seeding, the density fluctuation power between 30 and 70 kHz normalized to the WCM power increases monotonically (Fig. 8(b)). In fact, the power in this intermediate frequency range increases by a factor of three, which underlines the observation from Sec. II that the density fluctuations in this range react sensitively to seeding. The low frequency fluctuations (0 – 30 kHz, (a)) show an increase by a factor 2.5. Comparing the fluctuation powers of the N seeded discharge with the non-seeded reference, the one feature that sets the time traces clearly apart is the pronounced increase of intermediate frequency density fluctutations (30 – 70 kHz) in the seeded discharge, which is consistent with the observation from Fig. 2(g), where this increase is also observed in a mixed NBI- and ECRH-heated discharge. **It should be pointed out that during the N seeding phase, and therefore during the phase in which the density fluctuation levels increase, the divertor neutral density rises as well. To understand cause and effect of the flucutation increase during N seeding is one of the key topics to be understood. However, it is out of the scope of this paper and left for future work with dedicated experiments.**

Figure 8(e) shows the minimum of the edge radial electric field measured with active spectroscopy of He II and Doppler reflectometry. The comparably deep E_r minimum at around -15 kV/m is only established roughly 50 ms after the L-I transition. This minimum value of the E_r well is largely unchanged during the I-mode phase of the discharge, and its value indicates that the plasma was close to an I-H transition [27, 35, 64, 66]. The values from Doppler reflectometry

display a somewhat deeper minimum E_r in I-mode, but the general trend is comparable. The slight difference in $E_{r,\min}$ could be due to the phase velocity of the turbulence, which Doppler reflectometry would measure while He II spectroscopy would not. Hence, if the difference is due to a phase velocity effect, it would be a phase velocity pointing into the electron-diamagnetic direction. This is in line with recent theoretical work that ties the I-mode edge to drift-Alfvén turbulence and the dissipation of thermal energy by parallel conduction [37]. While the measurements from He II spectroscopy show a decrease of E_r starting at about 2.7 s, it is unclear whether this can be stated from Doppler reflectometry, especially considering the uncertainties. This potential loss of E_r well depth is concomitant with the loss in pedestal top T_e in Fig. 6(b). At 2.95 s, the I-L back transition occurs, followed by a further increase of $E_{r,\min}$ back to the L-mode value it showed before the I-mode started. It is interesting to note that the density fluctuation level between 30 and 70 kHz shortly after the loss of I-mode ($\sim$ 2.99 s) and with reduced edge E_r minimum is still at a low level. It increases abruptly only somewhat later. The turbulence level thus seems not to be directly related to the E_r well depth in I-mode, as is usually assumed for H-mode [73]. This supports the idea that the I-mode does not rely directly on the E_r shear, but is rather the consequence of phase randomization at large turbulence scales and a decrease in low-frequency density fluctuations connected to a transition from ion-temperature-gradient (ITG) dominated turbulence to Drift-Alfvén-turbulence [37].

It is unclear why the density fluctuation level at low frequencies increases as N is introduced into the private flux region. The effect is very robust and has been documented in all AUG I-mode plasmas with N seeding and in the C-Mod experiments [24]. Above, it has been pointed out that drift-Alfvén turbulence has been predicted as a key ingredient to the I-mode regime. This leads one to speculate that through seeding, the plasma edge is driven towards ITG dominated turbulence. Also recently, it has been shown in gyrokinetic simulations that the edge collisionality can lead to higher growth rates through the destabilition of resistive drift wave instabilities [74]. Since the collisionality depends linearly on the effective plasma charge, Z_{eff}, an increase in N content could have this effect. However, in the plasmas reported here, Z_{eff} increases by about 10%, which is not sufficient to cause significant changes in growth rate behavior. In contrast, high ion mass affects the parallel behavior of the drift wave instability such that transport may be reduced [75, 76], which is not the case here. The concomitant decrease of the energy confinement time with the increase of the low-frequency density fluctuation level and the eventual loss of the I-mode leads one to speculate that the N seeding does indeed change the pedestal properties of the I-mode plasmas.

However, a clear causality cannot be established with the present data. Furthermore, it should be noted that the energy confinement is strongly tied to temperature fluctuations. However, the plasma edge under investigation is optically thin for all cases, which makes correlation electron cyclotron emission measurements impossible to tie to electron temperature fluctuations.

IV. DISCUSSION

The demonstration of the compatibility of a confinement regime with detachment is of significance for the assessment of its application in a future fusion device. In that regard, the access to I-mode while the inner divertor leg is detached is an important finding. Nevertheless, demonstration of detachment of both divertor legs is still an open issue and is one of the directions of future I-mode research on ASDEX Upgrade.

The confinement loss as N is seeded into the discharge is not entirely understood at the moment. The increase of low frequency density fluctuations in the pedestal is a clear sign that the turbulence in the confinement region is affected by the boundary conditions set through the N seeding in the private flux region in the divertor. It is unlikely that the increase of N content in the edge plays a significant role, since the N density only increases marginally (cf Fig. 7(d)). The core radiation barely increases as measured by tomographic reconstruction of bolometer diagnostics. In order to clearly demonstrate if the increased energy transport is due to the pedestal turbulence, measurements of temperature fluctuations are necessary. In the discharges at hand, the optical thickness in the pedestal region is too low, therefore, measurements by the correlation electron cyclotron emission diagnostic are affected by density fluctuations. To put the present studies into context, it should be pointed out that N seeding into type-I ELMy H-mode plasmas generally can lead to a confinement improvement on AUG [31, 77], which is due to a reduction of the high field side high density (HFSHD) pattern through increased SOL radiation and a resulting inward shift of the density profile [78]. Since the HFSHD is a consequence of the direction of $E \times B$ drifts in the divertor in favorable configuration, it is usually not present in unfavorable configuration with reversed divertor drift directions. An outward shift of the density profile in non peeling-ballooning limited plasmas may lead to increased pedestal transport [79]. However, based on the present data, an outward shift can be ruled out.

The confinement loss through the seeding can indeed be compensated by additional auxiliary heating power input. To demonstrate this, Fig. 9 shows the β_{pol} signal from #37380, where I-

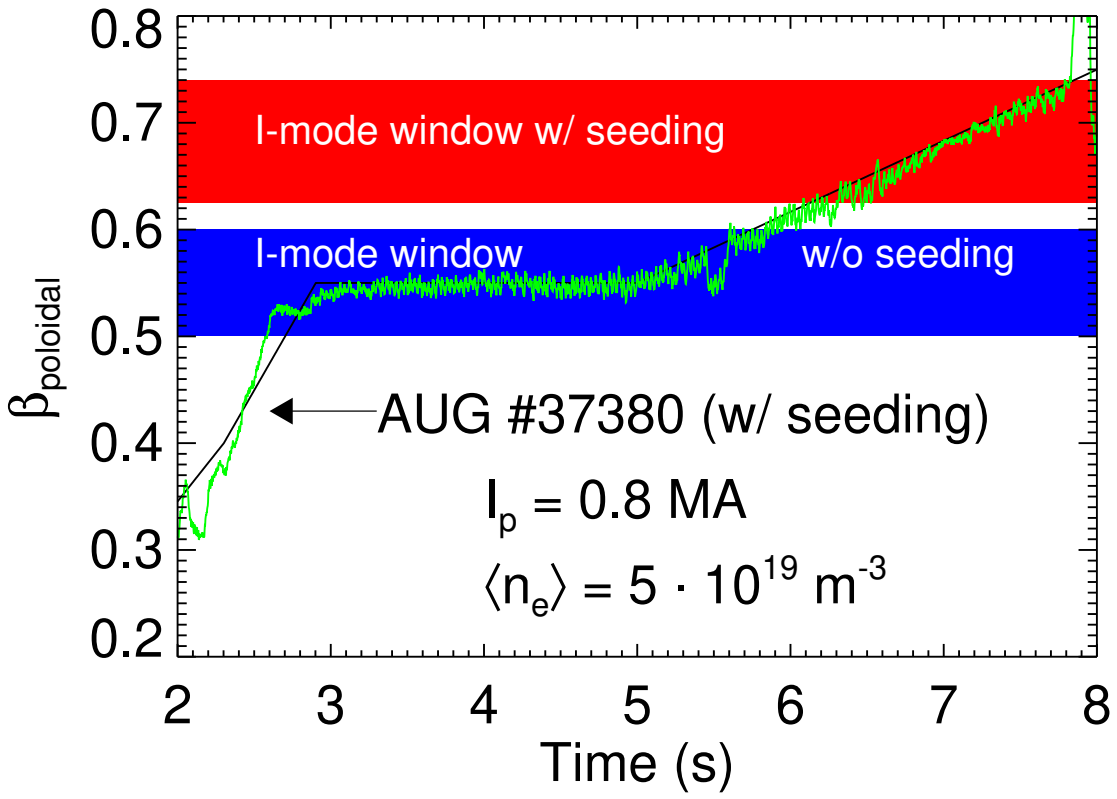

FIG. 9: Illustration of I-mode β_{pol} window shift due to N seeding. Non-seeded I-modes are accessed at values of $\beta_{\mathrm{pol}} \approx 0.5 - 0.6$, while the detached N-seeded I-mode ranges between $\beta_{\mathrm{pol}} \approx 0.63 - 0.74$ (for $I_p = 0.8\,\mathrm{MA}$ and $\langle n_e \rangle = 5 \times 10^{19}\,\mathrm{m}^{-3}$).

mode was obtained between 6.52 and 7.82 s. One observation that was an obstacle to finding the I-mode in N seeded discharges is that the I-mode existence window in β_{pol} appears to be shifted towards higher values. At these elevated values of β_{pol}, accessed with increased heating power, the confinement is at least as good as for non-seeded I-modes, with values of $H_{98}(y, 2) = 0.9$. In terms of a future fusion reactor, the required increased heating power is not desired, but future research is needed to assess if this effect can be mitigated.

V. CONCLUSIONS & OUTLOOK

Experiments on I-mode detachment in the ASDEX Upgrade tokamak have been reported. It is the first time that an I-mode plasma has been observed with a detached inner divertor leg. This result is important since it underlines the basic compatibility of I-mode operation together with detachment. In order to achieve detachment, nitrogen was seeded into the divertor, enabling

increased power dissipation, leading ultimately to the detachment of the inner strike point.

During N seeding at constant heating power, an increased low frequency density fluctuation level is observed in the plasma edge. At the same time, the thermal energy confinement decreases and eventually, the I-mode transitions back into an L-mode plasma. This effect cannot be mitigated solely by re-supplying the plasma energy via increased auxiliary heating power input. The I-mode with detached inner divertor is observed at elevated values of the plasma energy compared to non-seeded and attached I-modes. In order to access it, heating power in excess of typical heating powers required to access I-mode is necessary.

Future experiments will focus on the detachment of both divertor legs, either by increasing the N content together with increased auxiliary heating power, or by radiating some of the power flux in the plasma edge, e.g. by argon seeding. It seems likely that comparably moderate adjustments might be sufficient to detach both divertor legs due to the divertor power equipartition in unfavorable magnetic field configurations [80–85], where the amount of power arriving at the divertor legs is more balanced than in favorable configuration. Furthermore, the increased heating power requirements for N seeded I-modes should be better quantified in view of predictions towards future fusion devices.

Acknowledgments

Discussions during the preparation of this work with F. Reimold and C. Angioni are gratefully acknowledged. This work has been carried out within the framework of the EUROfusion Consortium and has received funding from the Euratom research and training programme 2014-2018 and 2019-2020 under grant agreement No 633053. The views and opinions expressed herein do not necessarily reflect those of the European Commission. Furthermore, this work is supported in part by US Department of Energy award DE-AC05-00OR22725.

---

[1] F. Wagner *et al.*, Phys. Rev. Lett. **49**, 1408 (1982).

[2] R. Wenninger *et al.*, Nucl. Fusion **54**, 114003 (2014).

[3] R. Pitts *et al.*, Nucl. Mat. Energy **20**, 100696 (2019).

[4] K. H. Burrell *et al.*, Phys. Plasmas **8**, 2153 (2001).

[5] F. Ryter *et al.*, Plasma Phys. Control. Fusion **40**, 725 (1998).

[6] D. G. Whyte *et al.*, Nucl. Fusion **50**, 105005 (2010).

[7] A. Marinoni *et al.*, Nucl. Fusion **55**, 093019 (2015).

[8] Y. Liu *et al.*, Nucl. Fusion **60**, 082003 (2020).

[9] Y. Takase *et al.*, Phys. Plasmas **4**, 1647 (1997).

[10] M. Greenwald *et al.*, Phys. Plasmas **6**, 1943 (1999).

[11] L. Gil *et al.*, Nucl. Fusion **60**, 054003 (2020).

[12] T. E. Evans *et al.*, Phys. Rev. Lett. **92**, 235003 (2004).

[13] A. W. Degeling *et al.*, Plasma Phys. Control. Fusion **45**, 1637 (2003).

[14] P. Lang *et al.*, Nucl. Fusion **44**, 665 (2004).

[15] T. Eich *et al.*, Phys. Rev. Lett. **107**, 215001 (2011).

[16] D. Brunner, B. LaBombard, A. Kuang, and J. Terry, Nucl. Fusion **58**, 094002 (2018).

[17] D. Silvagni *et al.*, Plasma Phys. Control. Fusion **62**, 045015 (2020).

[18] J. A. Goetz *et al.*, Phys. Plasmas **6**, 1899 (1999).

[19] A. Loarte *et al.*, Phys. Plasmas **18**, 056105 (2011).

[20] R. J. Goldston, M. L. Reinke, and J. A. Schwartz, Plasma Phys. Control. Fusion **59**, 055015 (2017).

[21] S. Potzel *et al.*, Nucl. Fusion **54**, 013001 (2014).

[22] O. Gruber *et al.*, Phys. Rev. Lett. **74**, 4217 (1995).

[23] A. Kallenbach *et al.*, Nucl. Fusion **55**, 053026 (2015).

[24] M. L. Reinke *et al.*, Nucl. Fusion **59**, 046018 (2019).

[25] A. Herrmann and O. Gruber, Fusion Sci. Technol. **44**, 569 (2003).

[26] A. Hubbard *et al.*, Nucl. Fusion **52**, 114009 (2012).

[27] T. Happel *et al.*, Plasma Phys. Control. Fusion **59**, 014004 (2017).

[28] F. Ryter *et al.*, Nucl. Fusion **57**, 016004 (2017).

[29] M. Kaufmann *et al.*, *Energy and Particle Control Characteristics of the ASDEX Upgrade LYRA Divertor* (17^{th} IAEA Fusion Energy Conference, Yokohama, Japan, 1998).

[30] T. Happel *et al.*, Nucl. Mat. Energy **18**, 159 (2019).

[31] A. Kallenbach, the ASDEX Upgrade Team, and the EUROfusion MST1 Team, Nucl. Fusion **57**, 102015 (2017).

[32] A. Loarte *et al.*, Nucl. Fusion **47**, S203 (2007).

[33] ITER Physics Expert Group on Confinement and Transport, ITER Physics Expert Group on Confinement Modelling and Database, and ITER Physics Basis Editors, Nucl. Fusion **39**, 2175 (1999).

[34] W. Suttrop, *Practical limitations to plasma edge electron temperature measurements by radiometry of electron cyclotron emission* (Max-Planck-Institute for Plasma Physics, IPP Report 1/306, Garching, Germany, 1997).

[35] M. Cavedon *et al.*, Nucl. Fusion **60**, 066026 (2020).

[36] P. Yushmanov *et al.*, Nucl. Fusion **30**, 1999 (1990).

[37] P. Manz *et al.*, Nucl. Fusion **60**, 096011 (2020).

[38] R. Neu *et al.*, J. Nucl. Mat. **313-316**, 116 (2003), plasma-Surface Interactions in Controlled Fusion Devices 15.

[39] A. E. Hubbard *et al.*, Phys. Plasmas **18**, 056115 (2011).

[40] I. Cziegler *et al.*, Phys. Plasmas **20**, 055904 (2013).

[41] P. Manz *et al.*, Nucl. Fusion **55**, 083004 (2015).

[42] A. Silva *et al.*, Rev. Sci. Instrum. **67**, 4138 (1996).

[43] J. C. Fuchs *et al.*, *Twodimensional reconstruction of the radiation power density in ASDEX Upgrade* (Proc. 21st EPS Conference on Plasma Physics, Montpellier, France, 1994), ECA Vol. 18B, 3, p. 1308.

[44] B. Sieglin *et al.*, Rev. Sci. Instrum. **86**, 113502 (2015).

[45] D. Nille, U. von Toussaint, B. Sieglin, and M. Faitsch, in *Bayesian Inference and Maximum Entropy Methods in Science and Engineering*, edited by A. Polpo *et al.* (Springer International Publishing, Cham, 2018), pp. 55–64.

[46] R. Fischer *et al.*, Fusion Sci. Technol. **58**, 675 (2010).

[47] B. Kurzan and H. D. Murmann, Rev. Sci. Instrum. **82**, 103501 (2011).

[48] E. Viezzer *et al.*, Rev. Sci. Instrum. **83**, (2012).

[49] R. M. McDermott *et al.*, Rev. Sci. Instrum. **88**, 073508 (2017).

[50] S. K. Rathgeber *et al.*, Plasma Phys. Control. Fusion **55**, 025004 (2013).

[51] R. M. McDermott *et al.*, Plasma Phys. Control. Fusion **60**, 095007 (2018).

[52] U. Plank, Rev. Sci. Instrum. (2020), *in preparation*.

[53] T. Happel *et al.*, Phys. Plasmas **22**, 032503 (2015).

[54] R. Sabot, P. Hennequin, and L. Colas, Fusion Sci. Technol. **56**, 1253 (2009).

[55] M. Hirsch *et al.*, Plasma Phys. Control. Fusion **43**, 1641 (2001).

[56] G. R. McKee *et al.*, Plasma Fus. Res. **2**, S1025 (2007).

[57] T. Estrada *et al.*, Plasma Phys. Control. Fusion **51**, 124015 (2009).

[58] H. W. Müller *et al.*, *Fluctuations, ELM Filaments and Turbulent Transport in the SOL at the Outer Midplane of ASDEX Upgrade* (IAEA, Daejon, Korea, 2010), report EXD/P3-23.

[59] E. Viezzer *et al.*, Nucl. Fusion **53**, 053005 (2013).

[60] K. Höfler *et al.*, Plasma Phys. Control. Fusion (2020), *submitted*.

[61] G. D. Conway *et al.*, Nucl. Fusion **46**, S799 (2006).

[62] L. Vermare *et al.*, Phys. Plasmas **18**, 012306 (2011).

[63] R. M. McDermott *et al.*, Phys. Plasmas **16**, 056103 (2009).

[64] T. Happel *et al.*, Nucl. Fusion **56**, 064004 (2016).

[65] T. M. Wilks *et al.*, *Access requirements for stationary ELM-suppressed pedestals in DIII-D and C-Mod H-mode and I-mode plasmas* (27$^{\text{th}}$ IAEA Fusion Energy Conference, Ahmedabad, India, 2018).

[66] P. Sauter *et al.*, Nucl. Fusion **52**, 012001 (2012).

[67] D. Prisiazhniuk *et al.*, Plasma Phys. Control. Fusion **59**, 025013 (2017).

[68] R. H. Kraichnan, Phys. Fluids **10**, 1417 (1967).

[69] M. G. Shats, H. Xia, and H. Punzmann, Phys. Rev. E **71**, 046409 (2005).

[70] P. Hennequin *et al.*, Plasma Phys. Control. Fusion **46**, B121 (2004).

[71] T. Happel *et al.*, Plasma Phys. Control. Fusion **59**, 054009 (2017).

[72] A. Kallenbach *et al.*, Nucl. Mat. Energy **18**, 166 (2019).

[73] H. Biglari, P. H. Diamond, and P. W. Terry, Phys. Fluids **2**, 1 (1990).

[74] N. Bonanomi *et al.*, Nucl. Fusion **59**, 126025 (2019).

[75] E. A. Belli, J. Candy, and R. E. Waltz, Phys. Rev. Lett. **125**, 015001 (2020).

[76] N. Bonanomi *et al.*, Phys. Plasmas (2020), *in preparation*.

[77] J. Schweinzer *et al.*, Nucl. Fusion **51**, 113003 (2011).

[78] M. G. Dunne *et al.*, Plasma Phys. Control. Fusion **59**, 014017 (2016).

[79] L. Frassinetti *et al.*, Nucl. Fusion **59**, 076038 (2019).

[80] A. Chankin, J. Nucl. Mat. **241**, 199 (1997).

[81] R. Pitts *et al.*, J. Nucl. Mat. **337-339**, 146 (2005), pSI-16.

[82] W. Fundamenski *et al.*, J. Nucl. Mat. **337-339**, 305 (2005), pSI-16.

[83] A. W. Leonard, Plasma Phys. Control. Fusion **60**, 044001 (2018).

[84] I. Paradela Pérez *et al.*, Nucl. Mat. Energy **19**, 531 (2019).

[85] I. Paradela Pérez *et al.*, Contrib. Plasma Phys. **60**, e201900166 (2020).